Micromechanical modelling of advanced ceramics

Patricia Alveen[1,*], Declan McNamara[1], Declan Carolan[1], Neal Murphy[1], Alojz Ivanković[1]

[1] School of Mechanical and Materials Engineering, University College Dublin, Ireland
* Corresponding author: Patricia.Alveen@ucdconnect.ie

Abstract

Advanced ceramics comprise a class of new materials finding increased application used in extreme conditions, such as high speed turning of aerospace alloys and rock drilling. Their high hardness makes them suitable for these applications, however their lower toughness means that premature failure due to fracture and chipping is still a major issue. Typically, they are composed of micron-sized particles of a primary hard phase together with a ceramic or metallic matrix.

A combined experimental-numerical method was used to investigate the role of microstructure on the fracture of these advanced ceramics. In particular, the effect of grain size and matrix content was examined. Representative finite volume (FV) microstructures were created using Voronoi tessellation. The cohesive zone parameters for the FV model were found experimentally using an adapted Three-Point-Bend (TPB) fracture toughness test method [1]. Image analysis was carried out on actual representative microstructures and compared to the FV microstructures to ensure that they were statistically similar.

It was found that the underlying microstructure significantly affects the fracture toughness of the advanced ceramic. Furthermore, it was found that by altering the microstructural parameters in the numerical model, such as grain size and binder content, it is possible to specify material improvements.

Keywords Advanced ceramics, microstructure, Voronoi tessellation, cohesive zone model

1. Introduction

In this study, we examine a two-phase ceramic structure composed of stiff hard particles together with a softer ceramic matrix material. Carolan et al [1, 2] have shown that the strength and toughness of polycrystalline materials are affected by both the grain size and matrix content. Therefore it is desirable to be able to virtually optimise these parameters to be able to produce stronger or tougher materials for specific applications. Current methods adopt a so-called "trial-and-error" approach to the design of new materials, which is both costly and time consuming. Hence, it is beneficial to be able to specify improvements to materials numerically. By specifying materials virtually, the influence of individual material parameters on the microstructural scale can easily be investigated and altered to change bulk material properties. In order to better model and predict material behaviour, the first step is the ability to produce statistically representative microstructures.

A number of authors [7–10] have generated finite element meshes directly based on actual microstructural images. In this work, however, a representative synthetically generated geometry is

produced, which is then compared to a real microstructure. Numerous studies have been carried out to produce numerical microstructures using Voronoi tessellation [11–13], with an emphasis on investigating stress distributions in plasticity [14–17] and fracture [18–20]. However there is little in the literature to show that numerical microstructures are actually representative of the real microstructures they were created to replace. This is important, especially in the case of fracture problems, where the morphology of a grain boundary interface is of added importance in initiating fracture. The present work attempts to produce numerical microstructures and subsequently compare them to these real microstructures to prove that they are statistically representative.

2. Synthetic microstructure generation

Voronoi tessellation was used to generate the geometrical model of the microstructure. It is a commonly used method for the generation of numerical microstructures of ceramic [19, 20] and metallic [11, 16, 21, 22] materials in both two- and three-dimensions. The Voronoi tessellation algorithm produces a random structure, which is representative of a polycrystalline material. A periodic microstructure was generated with periodic boundary conditions. To generate a dual interpenetrating phase microstructure, typical of some advanced ceramics, the Voronoi tessellation is applied. Each Voronoi tile is then reduced in area around the circumcentre of the tile until the desired area fraction of the second interpenetrating phase is reached, as shown in Figure 1.

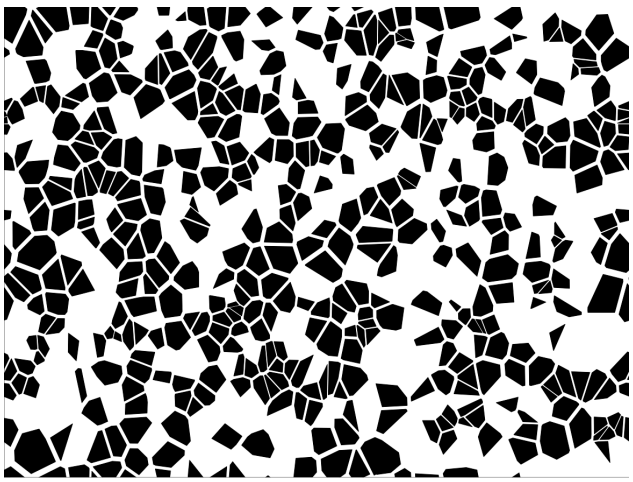

Figure 1: Numerically generated microstructure with 50% primary phase.

3. Results

3.1 Comparison of real and numerical microstructures

Grain size distribution, aspect ratio, percentage matrix agglomerations (MA) and percentage primary phase were obtained through image analysis. Matrix agglomerations are large regions containing no primary phase. From the image analysis it was found that the two real microstructures being investigated had an average areal primary phase content of 50.5% and 47.2% respectively. Four synthetic microstructures were generated for comparison, as shown in Figure 2. The generated microstructures all had a particle content in the range of 49-54%, which was close to the real

microstructures investigated. The percentage matrix agglomerations with respect to matrix phase content was calculated for the two real microstructures and was found to have an average value of 57.5% and 45.9% respectively. The two synthetic microstructures with matrix agglomerations, Figures 2b and 2d, had matrix agglomerations of 52.6% and 52.3% respectively.

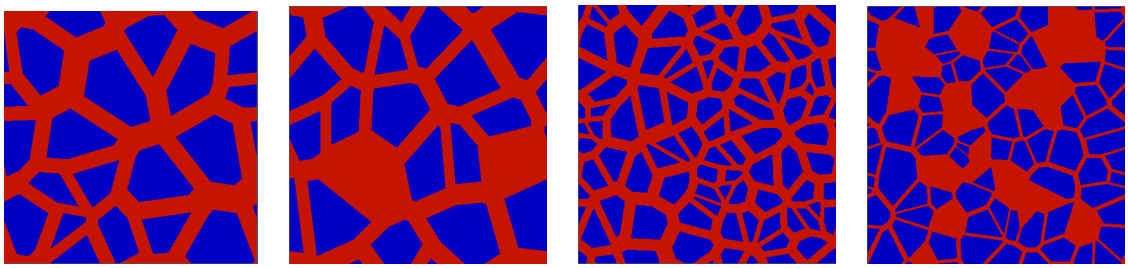

(a) 5×5 grains (b) 5×5 grains with MA (c) 10×10 grains (d) 10×10 grains with MA

Figure 2: Numerical microstructures used for finite volume

Grain size distribution, percentage particle phase and aspect ratio were obtained for both the numerical and corresponding real microstructures. A comparison between the two confirms that the numerical model is a good representation of the real microstructure, see Figures 3a and 3d. The grain size distribution of both the real and the numerical microstructure follow a log-normal distribution with a greater number of small grains, see Figure 3b and 3e. The real microstructure has a higher percentage of these small grains than its numerical counterpart due to small fragmented grains. However, it is not thought that these small fragments affect the mechanical properties of the bulk material. The aspect ratio of the real and the numerical microstructures show excellent agreement, as shown in Figure 3c and 3f. Visually it was also observed that the numerical microstructure resembled the real microstructure.

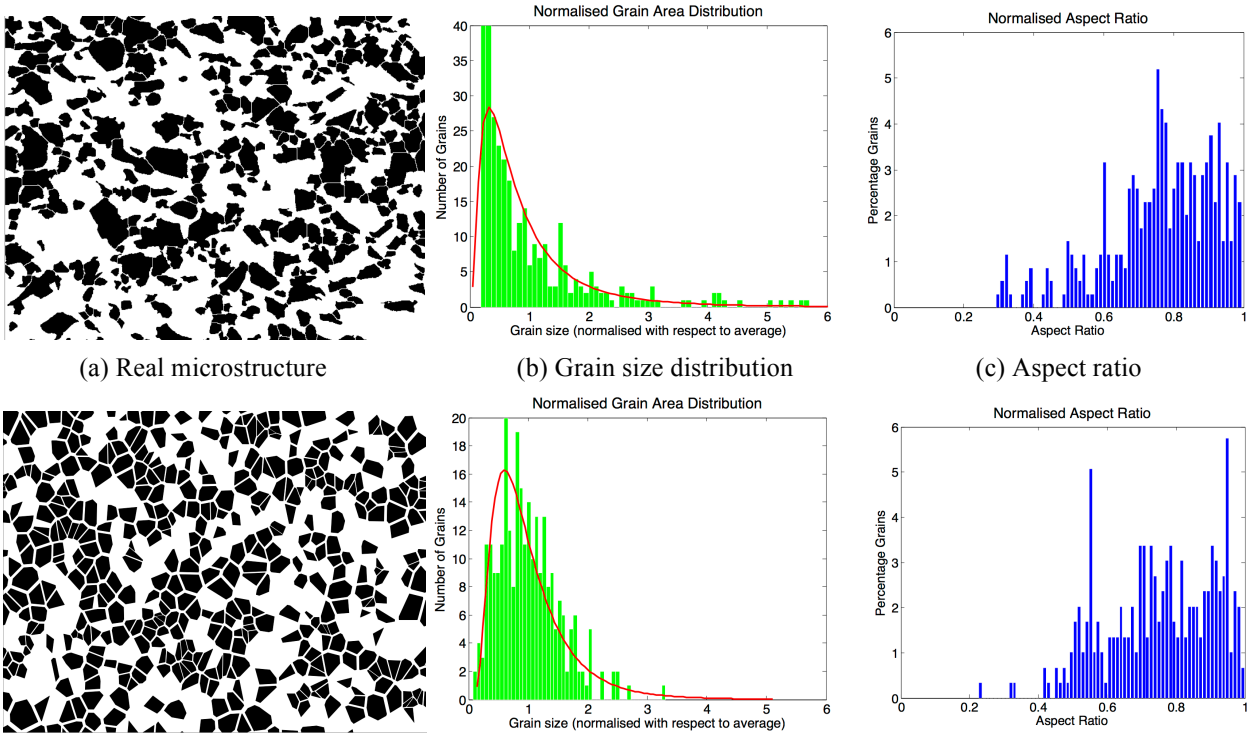

(a) Real microstructure (b) Grain size distribution (c) Aspect ratio

(d) Numerical microstructure (e) Grain size distribution (f) Aspect ratio

Figure 3: Comparison of real (a,b,c) and numerical (d,e,f) microstructures in terms of grain size distribution and aspect ratio.

3.2 Finite volume stress analysis

Finite volume based stress analysis was carried out on the four generated microstructures using OpenFOAM 1.6-ext [23]. Each generated microstructure was 100×100μm in size with approximately 50% particulates, but with varying grain sizes and matrix agglomerations, as shown in Figure 2. The simulations were 2-dimensional and plane strain was specified in the third direction. The Young's modulus and Poisson's ratio for the grains are 800 GPa and 0.1 respectively, while for the matrix material E = 300 GPa and ν = 0.1 were chosen for illustration. Both the particulates and matrix were treated as linear elastic over the course of the simulation. It should be noted that the elastic constants picked for each phase are not representative of any particular material.

The microstructures were subjected to a normal traction rate of 10 MPa/s in the y-direction for a total loading time of 10 seconds, while cyclic boundary conditions were applied in the x-direction, see Figure 4. The cyclic boundary conditions ensure that both material and displacement distribution are continuous from right to left. Furthermore, the 10×10 grain microstructures were increased to 200×200μm to investigate size effects.

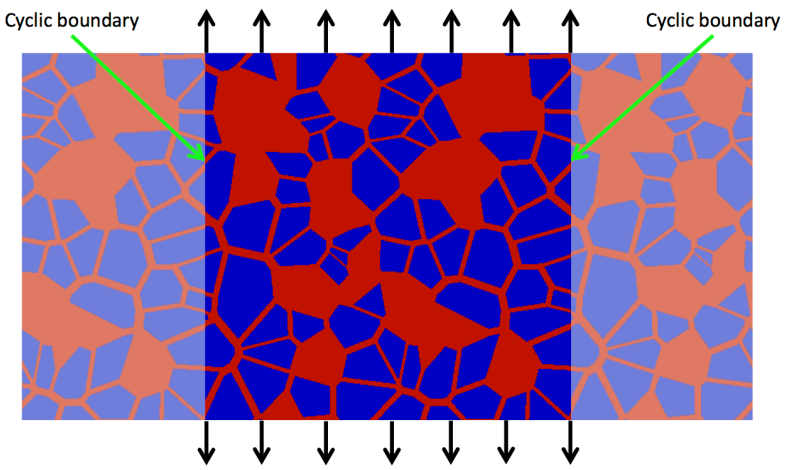

Figure 4: Generated microstructure with periodic boundary conditions subjected to a fixed traction

3.3 Effective elastic properties

The Young's Modulus value of a multiphase material depends on the properties of the individual phases. The upper and lower bounds for the elastic properties of the microstructures can be found using the Hashin-Shtrikman method from Eq. (1) and (2). The Hashin-Shtrikman bounds can be applied to transversely isotropic composites with arbitrary phase geometry [24–26].

$$k_l = k_2 + \frac{m_1}{\frac{1}{k_1-k_2}+\frac{m_2}{k_2+\mu_2}}, \quad k_u = k_1 + \frac{m_2}{\frac{1}{k_2-k_1}+\frac{m_2}{k_1+\mu_1}} \tag{1}$$

$$\mu_l = \mu_2 + \frac{m_1}{\frac{1}{\mu_1-\mu_2}+\frac{m_2(k_2+2\mu_2)}{2\mu_2(k_2+\mu_2)}}, \quad \mu_u = \mu_1 + \frac{m_2}{\frac{1}{\mu_2-\mu_1}+\frac{m_1(k_1+2\mu_1)}{2\mu_1(k_1+\mu_1)}} \tag{2}$$

Where *l* and *u* represent the upper and lower bounds respectively, k is the bulk modulus, μ is the shear modulus, m is the volume fraction and *1* and *2* represent the two phases in the material.

$$E = \frac{9k_i\mu_i}{3k_i+\mu_i} \tag{3}$$

$$\nu = \frac{3k_i-2\mu_i}{6k_i+2\mu_i} \tag{4}$$

The upper and lower bounds for the Young's modulus and Poisson's ratio can then be calculated from Eq. (3) and (4) respectively [21], by letting i equal u and l from Eq. (1) and (2). Using the Hashin-Shtrikman method the Young's modulus bounds for 50% particulates was found to be 459.9-480.6 GPa (Table 1).

The Eshelby-Mori-Tanaka approach [27–29] for determining the elastic properties of composites containing randomly oriented inclusions was also employed in the current work. Using this approach, and treating the inclusions as circular, i.e. an aspect ratio of one, the ratio of bulk modulus, k, and shear modulus, μ of a composite material to that of the matrix can be written as:

$$\frac{k}{k_m} = \frac{1}{1+V_f p} \tag{5}$$

$$\frac{\mu}{\mu_m} = \frac{1}{1+V_f q} \tag{6}$$

where k_m, μ_m and V_f are the bulk modulus of the matrix, shear modulus of the matrix and volume fraction of the inclusion respectively, and p and q are parameters derived from the Eshelby tensor and defined in Tandon and Weng [27]. Using the Eshelby-Mori-Tanaka method, the Poisson's ratio was found to be 0.114 for all the microstructures.

The effective stress, σ^e, and strain, ε^e, were found by averaging the local stress and strain in each cell using Eq. (7) and (8) [30]. This is known as homogenisation.

$$\sigma^e = \frac{1}{V_\Omega}\int_{V_\Omega} \sigma \, dV \tag{7}$$

$$\varepsilon^e = \frac{1}{V_\Omega}\int_{V_\Omega} \varepsilon \, dV \tag{8}$$

Where V_Ω is the total volume of integration. These values were then used to calculate the effective Young's Modulus E^e from

$$E^e = \frac{1}{\varepsilon^e_{yy}}[\sigma^e_{yy} - \nu^e(\sigma^e_{xx} + \sigma^e_{zz})] \tag{9}$$

where the effective Poisson's ratio, ν^e, is

$$\nu^e = \frac{\sigma^e_{xx}}{\sigma^e_{yy} + \sigma^e_{zz}} \tag{10}$$

The effective Young's modulus, $E_{Eq.9}$ of the microstructures is as shown in Table 1. The Poisson's ratio was found to be 0.112 for all the microstructures. The Young's modulus was also determined by calculating the average tractions and strains on the loading boundaries. Using these values the stress, σ, and strain, ε, and hence the Young's Modulus, E, could be calculated by:

$$\sigma^e = \frac{F_1}{L_1 t} \tag{11}$$

$$\varepsilon^e = \frac{u_1}{L_2} \tag{12}$$

$$E^e = \frac{\sigma^e}{\varepsilon^e} \tag{13}$$

Where F_1 is the loading force on the prescribed boundary, L_1 and L_2 are the width and height of the specimen, t is the thickness of the specimen and u_1 is the displacement of the sample along the loading direction. The Young's modulus value calculated using Eq. (13), was found to be higher than the value calculated using the average volumes (Table 1).

Table 1: Elastic properties of numerical microstructures where $E_{Eq.9}$ is calculated using the homogenisation method in Eq. (9), $E_{Eq.13}$ is calculated using the load-displacement method in Eq. (13), E_{EMT} is calculated using the Eshelby-Mori-Tanaka method, and E_{HS} is calculated using the Hashin-Shtrikman method

Microstructure	V_f	$E_{Eq.9}$ **(GPa)**	$E_{Eq.13}$ **(GPa)**	E_{EMT} **(GPa)**	E_{HS} **(GPa)**
5×5	0.5	463.2	475.9	462.1	459.6 - 480.6
10×10	0.5	463.3	476.3	462.1	459.6 - 480.6
5×5 with MA	0.49	459.7	472.4	457.7	455.3 - 476.1
10×10 with MA	0.54	485.1	498.6	484.7	477.4 - 499.8
10×10 (200×200μm)	0.5	463.3	476.3	462.1	459.6 - 480.6
10×10 with MA (200×200μm)	0.54	485.1	498.6	484.7	477.4 - 499.8

The Young's modulus value for the two microstructures with no matrix agglomerations was found to be very similar using all the methods for calculating the Young's modulus. This suggests that the Young's modulus is not affected by the grain size. It was also observed that increasing the specimen size to 200×200μm did not change the Young's modulus value showing that it is not size dependent. Furthermore, the matrix agglomerations were not found to affect the Young's modulus values. Only the volume fraction of particles was found to make a difference.

It was found that the load-displacement method consistently gave higher results than both the Eshelby-Mori-Tanaka and the homogenisation methods. The load-displacement values were found to lie close to the upper bounds of the Hashin-Shtrikman limits. The homogenising was found to give realistic values for Young's modulus and Poisson's ratio, and these values were found to be in good agreement with the Eshelby-Mori-Tanaka method. Both these values tend to lie close to the lower bound of the Hashin-Shtrikman limits.

Figures 5a and 5b plot the distribution of Von-Mises equivalent strain for a 5×5 and 10×10 microstructure with no matrix agglomerations. Figures 5c and 5d plot the distribution of Von-Mises

equivalent stress for the same two microstructures. Similarly Figures 6a and 6b plot the Von-Mises equivalent strain for a 5×5 and 10×10 microstructure with matrix agglomerations and Figures 6c and 6d plot the corresponding Von-Mises stresses. From Figure 5 it may be observed that the distribution of local stress and strain does not vary significantly between the two microstructures, showing that stress and strain are not size dependent. However, when comparing Figure 5 and 6, it can be observed that the matrix agglomerations do affect the local distribution of stress and strain in the microstructure, with higher stress and strain being detected near the agglomerations. The highest stresses are seen in the hard phase at the phase interface, while the highest strains are seen in the more compliant matrix phase. This shows that matrix agglomerations in the microstructure act as stress concentration factors. Carolan has previously observed this effect in the context of dynamic fracture of advanced ceramics [31].

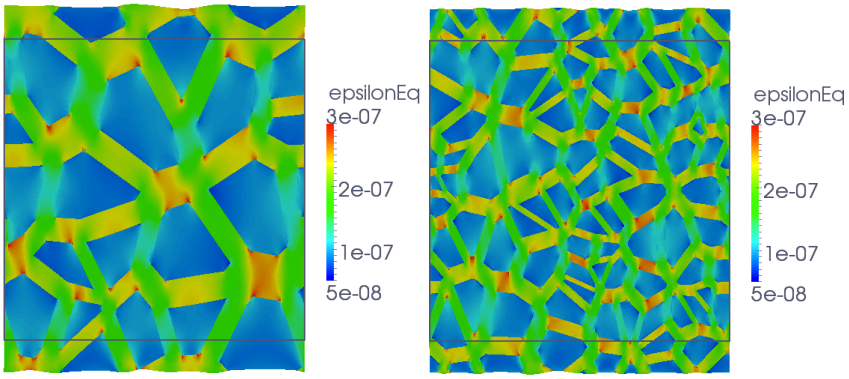

(a) 5x5 grains strain (b) 10x10 grains strain

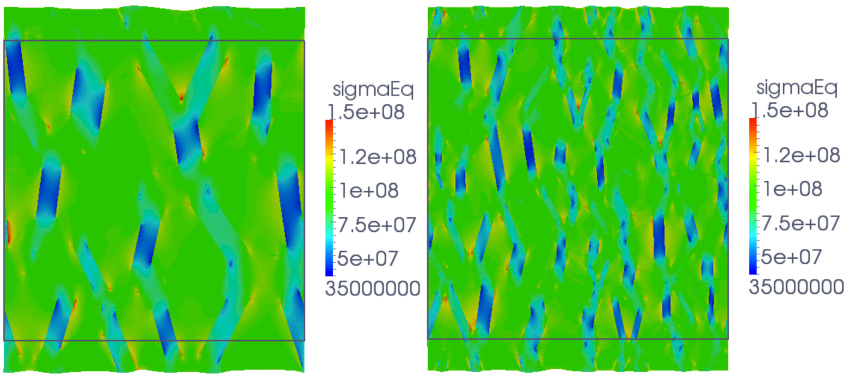

(c) 5×5 grains stress (d) 10×10 grains stress

Figure 5: Strain and stress distribution in the numerical microstructures with no matrix agglomerations subjected to a normal traction of 100 MPa. The deformation of the microstructure is magnified by a factor of 1000.

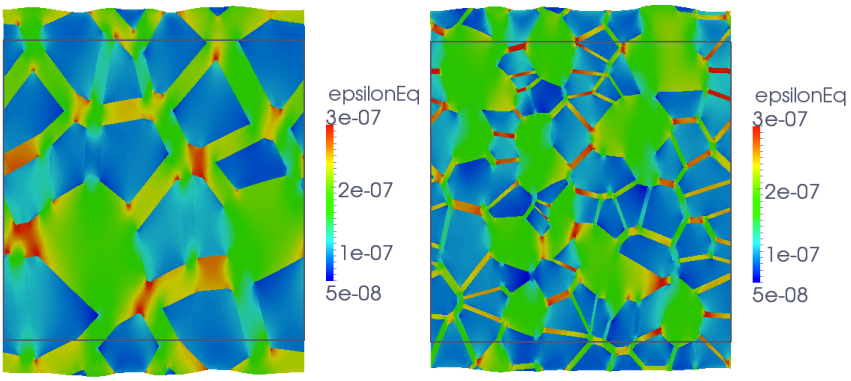

(a) 5×5 grains strain (b) 10×10 grains strain

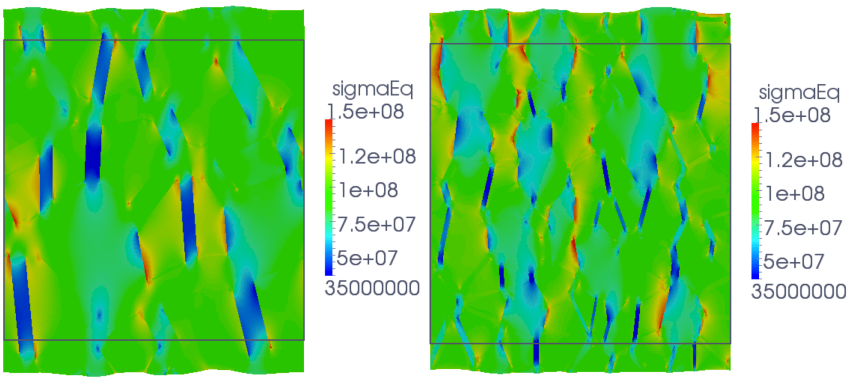

(c) 5×5 grains stress (d) 10×10 grains stress

Figure 6: Strain and stress distribution in the numerical microstructures with matrix agglomerations subjected to a normal traction of 100 MPa. The deformation of the microstructure is magnified by a factor of 1000.

4. Conclusion

The purpose of this paper was to develop statistically representative numerical models of advanced ceramic microstructures. The microstructures were generated using the Voronoi tessellation algorithm and subsequently altered to add a specified percentage primary inclusion phase and secondary phase matrix agglomerations to the microstructure. In the current paper it has been shown that the Voronoi Tessellation technique is a good method for the production of synthetic microstructures. The synthetic microstructures were compared to true microstructures and were found to be statistically representative in terms of grain size distribution, aspect ratio and agglomeration of a second phase material.

Using the numerically generated microstructures, Finite Volume analysis was carried out to investigate the stress and strain distributions in the microstructures and hence calculate the effective Young's modulus and Poisson's ratio. It was observed that the higher strains occur in the more compliant second phase material. This was more prevalent when there were agglomerations of the second phase material. Furthermore, it was observed that the presence of matrix agglomerations act as a stress concentration factor. Hence, the interface between particulates and a matrix agglomeration is likely to be the source of failure. This emphasises the need for accurate representation of microstructures in a numerical model.

The current paper presents a useful and implementable tool for investigating the effect of microstructural parameters on the microscopic stress distribution in a polycrystalline material. It is intended that the work will be extended to include other types of advanced ceramic material including single-phase ceramic as well as complex structures containing many different phases. Future work will concentrate on comparing the bulk elastic predictions with experimentally determined values for a range of advanced ceramics. It is also intended to extend the predictive capabilities of the models to capture strength and fracture behaviour.

Acknowledgements

The authors would like to thank Element Six Ltd., Enterprise Ireland and the Irish Research Council for providing financial support for this research.

References

[1] D. Carolan, P. Alveen, A. Ivanković, N. Murphy. Effect of notch root radius on fracture toughness of polycrystalline cubic boron nitride. Eng. Fract. Mech., 78 (2011) 2885-2895

[2] D. Carolan, A. Ivanković, N. Murphy. Thermal shock resistance of polycrystalline cubic boron nitride. J. Eur. Ceram. Soc., 32 (2012) 2581–2586

[3] J.J. Friel, J.C. Grande, D. Hetzner, K. Kurzydlowski, D. Laferty, M.T. Shehata, V. Smolej, G.F. Van-der Voort, L. Wojnar. Practical Guide to Image Analysis. ASM International, 2000.

[4] J.C. Russ. The Image Processing Handbook. CRC Press, 2nd edition, 1995.

[5] W.S. Rasband. ImageJ. U.S. National Institute of Health, Bethesda, Maryland, USA, http://imagej.nih.gov/ij/, 1997-2012.

[6] MATLAB. Image Processing Toolbox. The MathWorks Inc., Natick, Massachusetts.

[7] S.A. Langer, E.R. Fuller Jr., W.C. Carter. OOF: An Image-Based Finite-Element Analysis of Materials Microstructures. Comput. Sci. Eng., May/June (2001) 15–23

[8] V.R. Coffman, A.C.E. Reid, S.A. Langer, G. Dogan. OOF3D: An image-based finite element solver for materials science. Math. Comput. Simul. (2012) (http://dx.doi.org/10.1016/j.matcom.2012.03.003)

[9] A.C.E. Reid, S.A. Langer, R.C. Lua, V.R. Coffman, S. Haan, R.E. García. Image-based finite element mesh construction for material microstructures. Comput. Mater. Sci., 43(4) (2008) 989-999

[10] M. Huang, Y. Li. X-ray tomography image-based reconstruction of microstructural finite element mesh models for heterogeneous materials. Comput. Mater. Sci., 67 (2012) 63–72

[11] M. Nygårds, P. Gudmundson. Three-dimensional periodic Voronoi grain models and micromechanical FE-simulations of a two- phase steel. Comput. Mater. Sci., 24 (2002) 513–519

[12] M. Kühn, M.O. Steinhauser. Modeling and simulation of microstructures using power diagrams: Proof of the concept. Appl. Phys. Lett., 93 (2008) 034102

[13] L. Madej, L. Rauch, K. Perzynski, P. Cybulka. Digital Material Representation as an efficient tool for strain inhomogeneities analysis at the micro scale level. Archives of Civil and Mechanical Engineering, XI(3) (2011) 661–679

[14] P Zhang, D Balint, J Lin. An integrated scheme for crystal plasticity analysis: Virtual grain

structure generation. Comput. Mater. Sci., 50 (2011) 2854–2864

[15] P. Zhang, M. Karimpour, D. Balint, J. Lin, D. Farrugia. A controlled Poisson Voronoi tessellation for grain and cohesive boundary generation applied to crystal plasticity analysis. Comput. Mater. Sci., March (2012) 2–7

[16] R. Dobosz, M. Lewandowska, K.J. Kurzydlowski. FEM modelling of the combined effect of grain boundaries and second phase particles on the flow stress of nanocrystalline metals. Comput. Mater. Sci., 53(1) (2012) 286–293

[17] M. Danielsson, D.M. Parks, M.C. Boyce. Micromechanics, macromechanics and constitutive modeling of the elasto-viscoplastic deformation of rubber-toughened glassy polymers. J. Mech. Phys. Solids, 55(3) (2007) 533–561

[18] H.D. Espinosa, P.D. Zavattieri. A grain level model for the study of failure initiation and evolution in polycrystalline brittle materials. Part I: Theory and numerical implementation. Mech. Mater., 35 (2003) 333–364

[19] D.H. Warner, J.F. Molinari. Micromechanical finite element modeling of compressive fracture in confined alumina ceramic. Acta Mater., 54(19) (2006) 5135–5145

[20] T. Zhou, C. Huang, H. Liu, J. Wang, B. Zou, H Zhu. Crack propagation simulation in microstructure of ceramic tool materials. Comput. Mater. Sci., 54 (2012) 150–156

[21] H. Li, K. Li, G. Subhash, L.J. Kecskes, R.J. Dowding. Micromechanical modeling of tungsten-based bulk metallic glass matrix composites. Mater. Sci. Eng., A, 429 (2006) 115–123

[22] Y. Wang, L. Shuhua, P. Xiao, J. Zou. FEM simulations of tensile deformation and fracture analysis for CuW alloys at mesoscopic level. Comput. Mater. Sci., 50 (2011) 3450–3454

[23] H. Weller, G. Tabor, H. Jasak, C. Fureby. A tensorial approach to CFD using object oriented techniques. Computers in Physics, 12 (1998) 620– 631

[24] Z. Hashin, S. Shtrikman. A variational approach to the theory of the elastic behaviour of multiphase materials. J. Mech. Phys. Solids, 11 (1963) 127–140

[25] P. Wall. A comparison of homogenization, Hashin-Shtrikman bounds and the Halpin-Tsai equation. Applications of Mathematics, 42 (1997) 245–257

[26] Z. Hashin. On elastic behaviour of fibre reinforced materials of arbitrary transverse phase geometry. J. Mech. Phys. Solids, 13 (1965)119–134

[27] G. P. Tandon and G. J. Weng. Average stress in the matrix and effective moduli of randomly oriented composites. Compos. Sci. Technol., 27 (1986) 111–132

[28] T. Mori and K. Tanaka. Average stress in matrix and average elastic energy of materials with misfitting inclusions. Acta Metall., 21 (1973) 571– 574

[29] J.D. Eshelby. The determination of the elastic field of an ellipsoidal inclusion, and related problems. Proc. R. Soc. London, Ser. A, 241 (1957) 376–396

[30] X. Chen, Y. Mai. Micromechanics of rubbertoughened polymers. J. Mater. Sci., 33 (1998) 3529–3539

[31] D.Carolan, Mechanical and fracture properties of polycrystalline cubic boron nitride as a function of rate and temperature, PhD Thesis, University College Dublin, 2011.